Universal spectral statistics in Wigner-Dyson, chiral and Andreev star graphs II: semiclassical approach

Sven Gnutzmann[1, ∗] and Burkhard Seif[2, †]

[1]Institut für Theoretische Physik, Freie Universität Berlin, Arnimallee 14, 14195 Berlin, Germany
[2]Institut für Theoretische Physik, Universität zu Köln, Zülpicher Str. 77, 50937 Köln

A semiclassical approach to the universal ergodic spectral statistics in quantum star graphs is presented for all known ten symmetry classes of quantum systems. The approach is based on periodic orbit theory, the exact semiclassical trace formula for star graphs and on diagrammatic techniques. The appropriate spectral form factors are calculated upto one order beyond the diagonal and self-dual approximations. The results are in accordance with the corresponding random-matrix theories which supports a properly generalized Bohigas-Giannoni-Schmit conjecture.

I. INTRODUCTION

Since Bohigas, Giannoni and Schmit conjectured in their in a seminal paper [1] that the spectral fluctuations in quantum systems with a chaotic classical counterpart follow the predictions of the Gaussian random-matrix ensembles GUE, GOE, or GSE (depending on the behavior of the system under time-reversal and spin rotations) a lot of numerical data has been gathered that strongly support this conjecture (see [2, 3] and references therein). While an analytic proof of the conjecture and a precise statement of its limits is still lacking there has been a continuous advance in understanding the universality of spectral statistics. The main tool in the semiclassical approach is Gutzwiller's trace formula [4] which expresses the fluctuating part of the density of states as a sum over classical periodic orbits. The main object of interest is the spectral form factor which is the Fourier transform of the spectral two-point correlation function (below we will call this the second-order form factor) which is expressed semiclassically via the trace formula as a sum over pairs of periodic orbits which share the same action. In the diagonal approximation introduced by Berry [5] only those pairs for which both periodic orbits are either equal or the time-reverse of the other are summed over. The assumption of hyperbolic chaos is then sufficient to prove that the leading linear order in a short-time expansion for a quantum system follows the random-matrix predictions. Recently Sieber and Richter [6] started new progress for a semiclassical approach beyond the diagonal approximation with the observation that self-crossing trajectories in a billiard of constant negative curvature have a partner orbit of the same action that avoids this self-crossing. In the form factor these Sieber-Richter pairs give the quadratic order in time as predicted by the GOE. Their approach has been generalized to general hyperbolic billiards [7] and later in a phase space approach

to hyperbolically chaotic Hamiltonian systems with two [8, 9] and finally any number of degrees of freedom [10]. Finally, the cubic order in the short-time expansion has been calculated [11].

The first non-vanishing order in τ is known as the *diagonal approximation* in the Wigner-Dyson classes which is linear in τ. For the chiral and Andreev classes the first non-vanishing order is τ^0 and has been called *the self-dual approximation* [12]. So far the fidelity to the predictions of Gaussian random-matrix theory has been derived for the classes C and CI – here, we will give a complete account of for star graphs in all symmetry classes. Though we restrict to graphs here, the following calculation show what types of periodic orbits and which of their properties are responsible for universality in more general Hamiltonian system.

The next to leading order (the *weak localization corrections*) will also be calculated for all ten ensembles of star graphs. For fully connected Wigner-Dyson graphs in class AI (GOE) these have recently been calculated to order τ^3 (based on much earlier work on τ^2) by Berkolaiko *et al* [13]. These authors generalized the Sieber-Richter approach to graphs and introduced diagrammatic techniques similar to those used in this paper. The relation between the corresponding expansion for quantum systems in class AII (GSE) and the AI (GOE) expansion has been considered receltly [14, 15].

The corresponding ensembles of star graphs have been constructed in the first paper of this series [16]. Each of these ensembles obeys the symmetry conditions of one class in the ten-fold classification of quantum systems. There, we have also introduced the first-order and second-order spectral form factors as the Fourier transforms of the fluctuating part of the density of states and the two-point correlation function and related them to them to the scattering matrix if the star graphs via an exact semiclassical trace formula. We have also shown numerically that these spectral form factors follow the predictions of the corresponding Gaussian random-matrix ensembles. The second-order form factor of graphs in the Wigner-Dyson classes follow the predictions of the well-known Wigner-Dyson ensembles GUE, GOE, GSE.

∗Electronic address: sven@gnutzmann.de
†Electronic address: bseif@thp.uni-koeln.de

For the remaining seven "novel" symmetry classes the first-order form factor for star graphs coincides with the corresponding Gaussian random-matrix prediction. For the novel ensembles the fidelity to Gaussian random-matrix prediction is the content of a properly generalized Bohigas-Giannoni-Schmit conjecture [16].

The (generalized) Bohigas-Giannoni-Schmit conjecture states that the spectral fluctuations of a *single* classically chaotic physical system follow the predictions of Gaussian random-matrix theories. Here, we have explicitly introduced *ensembles* of star graphs. It has been shown however [17] that ensemble averages over certain phases in graphs are equivalent to a spectral average of a *single* spectrum in a graph with incommensurate bond lengths.

For the first-order form factor for chiral and Andreev star graphs the generalized Bohigas-Giannoni-Schmit conjecture is slightly weaker in as much as not a single spectrum is conjectured to follow the random-matrix predictions but a one-parameter average over different values of an effective $\hbar$ (an average over different values of the Fermi level or different quantizations of the same system). We leave it open here to what extend the ensemble averages for the graphs in the novel symmetry classes are equivalent to such a one-parameter average.

In section II we introduce the diagrammatic representation of the form factors: the section starts with a general description in II A, there we give the vertex ("d-vertex") and bond ("line") contributions to a diagram for each of the ten symmetry classes in II B and also give the diagrammatic expansion of the ensemble averaged form factors in II C. In section III we calculate the diagonal and self-dual approximations and one order beyond for the form factors of the ten ensembles: this section first introduces a systematic diagrammatic short-time expansion of the form factors in III A and then explicitly gives all diagrams of the leading and next-to-leading order which are calculated explicitly in III B.

II. THE DIAGRAMMATIC REPRESENTATION OF FORM FACTORS FOR STAR GRAPHS

Star graphs are simple quantum systems with an exact semiclassical trace formula for the density of states [18]. They consist of V vertices connected by B bonds of length L_i. A particle propagates freely on the bond and is scattered at the vertices according to prescribed unitary vertex scattering matrices.

In a star graph B bonds emanate from one central vertex and connect it to B peripheral vertices [16, 18, 19]. We have generalized previous star graph models by allowing for a wave function with μ components. In our model all bonds have the same length and the free propagation along the bonds and the scattering at the central vertex do not mix the components (but have to obey some symmetry conditions). The central vertex scattering is thus a unitary $\mu B \times \mu B$ matrix of the form

$\mathcal{S}_{C,\alpha j,\alpha',j'} = \delta_{\alpha\alpha'}\mathcal{S}_{C,jj'}^{(\alpha)}$ [16]. Here, $j,j' = 1,\ldots,B$ is an index for the bonds and $\alpha,\alpha' = 1,\ldots,\mu$ counts the wave function components. In addition, propagation along the bonds and the central scattering are time-reversal invariant. The proper choice of the scattering process at the peripheral vertices fixes the symmetry class (and breaks time-reversal if necessary). All peripheral scattering processes can be described by a single unitary $\mu B \times \mu B$ matrix of the form $\mathcal{S}_{P,\alpha j,\alpha',j'} = \delta_{jj'}\sigma_{\alpha\alpha'}^{(j)}$ [16]. For graphs in the novel symmetry classes this process involves an equivalent of *Andreev scattering* (electron-hole conversion).

A. Diagrammatic representation of the form factors

Prescribing the central and peripheral scattering vertex matrices $\mathcal{S}_C$ and $\mathcal{S}_P$ leads to a quantization of the graph. Their product is the reduced bond scattering matrix $\mathcal{S}_B \equiv \mathcal{S}_P\mathcal{S}_C$. The density of states is represented exactly by the semiclassical trace formula

$$d(\kappa) = 1 + \frac{2}{\mu B}\,\mathrm{Re}\sum_{n=1}^{\infty}\mathrm{e}^{\mathrm{i}2\pi\kappa\frac{gn}{\mu B}}s_n. \tag{1}$$

Here, κ is the wave number in units of the (macroscopic) mean level spacing and

$$s_n = \mathrm{tr}\,\tilde{\mathcal{S}}_B^n = \sum_{j_i,\alpha_i}\sigma_{\alpha_1\alpha_n}^{(j_1)}\mathcal{S}_{C,j_1j_n}^{(\alpha_n)}\ldots\sigma_{\alpha_2\alpha_1}^{(j_2)}\mathcal{S}_{C,j_2j_1}^{(\alpha_1)} \tag{2}$$

is the trace of the n-th power of the reduced bond scattering matrix. The latter may be represented by diagrams [13]

$$s_n = \tag{3}$$

In order to distinguish between a bond or vertex in a star graph and in a diagram we will use the terms *lines* and *d-vertices* for the diagrams and reserve *bonds* and *vertices* for star graphs. The d-vertices in the above diagram correspond to the peripheral vertices in the star graph which are visited one after another. Each d-vertex contributes a factor

$$= \sigma_{\alpha\alpha'}^{(j)} \equiv \mathcal{S}_{P,j\alpha,j'\alpha'} \tag{4}$$

to the diagram. This describes the scattering of a particle that moves outwards on bond j in the state α' to a particle moving inwards on the same bond in state α.

The lines in the diagram carry a factor

$$\begin{array}{c} \bullet\, j \\ \big\uparrow\, \alpha \\ \bullet\, j' \end{array} = \mathcal{S}_{C,jj'}^{(\alpha)} \equiv \mathcal{S}_{C,\,j\alpha,j'\alpha}. \qquad (5)$$

A diagram is calculated by summing over all indices all indices $j_k = 1,\dots,B$ and $\alpha_k = 1,\dots,\mu$ – obviously for (3) one arrives back at (2). We have defined the first-order form factor [16] as the Fourier transform of the (ensemble averaged) fluctuating part of the density of states. The first-order form factor in discrete time $\tau = \frac{gn}{\mu B}$ ($g = 2$ in classes AII, DIII, and CII which have Kramers' degeneracy, else $g = 1$) is upto a constant given by the ensemble average

$$K_{1,n} = \frac{2}{g}\,\langle s_n \rangle. \qquad (6)$$

After an additional time average (over a small interval $\Delta n \ll B$) which is needed for comparison with random-matrix theory the first-order form factor (in continuous time) is $K_1(\tau = \frac{gn}{\mu B}) = \frac{1}{\Delta n}\sum_{n'=n}^{n+\Delta n-1} K_{1,n}$. Equivalently there is a discrete and continuous time second-order form factors. In the Wigner-Dyson case they are given by

$$\begin{aligned} K_{2,n} &= \tfrac{1}{B}\,\langle s_n s_n^* \rangle \\ &= \tfrac{1}{B}\left\langle \vcenter{\hbox{}} \right\rangle \end{aligned} \qquad (7)$$

and $K_2(\tau = \frac{gn}{\mu B}) = \frac{1}{\Delta n}\sum_{n'=n}^{n+\Delta n-1} K_{2,n}$. In the diagram for s_n^* we have indicated the complex conjugation by dashed lines. Most contributions to s_n and $|s_n|^2$ do not survive the ensemble average. The remaining contributions can be written as a sum over various diagrams involving the same lines and d-vertices but have less summation indices. This expansion will be explained in section II C.

B. The line and d-vertex factors for the ten symmetry classes

In the previous section we have not specified the central and peripheral scattering matrices for the different symmetry classes. Let us now give the explicit d-vertex factors and line factors for each of the ten symmetry classes that are equivalent to the construction in [16]. The lines in the diagram correspond to the central scattering process. In our model each components of the wave function is either scattered in the center by the $B \times B$ discrete Fourier transform matrix $\mathcal{S}_{DFT,kl} = \frac{1}{\sqrt{B}}e^{i2\pi\frac{kl}{B}}$ or by its

complex conjugate for which we will use the lines

$$\begin{array}{c}\bullet\,j\\ \big\uparrow\\ \bullet\,j'\end{array} = \frac{1}{\sqrt{B}}e^{2\pi i\frac{jj'}{B}} \quad \text{and} \quad \begin{array}{c}\bullet\,k\\ \big\uparrow\\ \bullet\,k'\end{array} = \frac{1}{\sqrt{B}}e^{-2\pi i\frac{kk'}{B}}. \quad (8)$$

For some classes the line carries an additional index for the component of the wave function – the line factor however does not depend on it.

In the Wigner-Dyson classes only full lines exist in the representation of s_n while there are only dashed lines in s_n^*. The wave-function has only one component in class AI. It has two components in class A which we will call "spin up" with the symbol $\uparrow$ and "spin down" with the symbol $\downarrow$ for conveveniences. Finally, it has a four components in class AII – in addition to the spin labels $\uparrow, \downarrow$ we use the symbols $\Uparrow, \Downarrow$ and call the latter "iso-spin" up and down for convenience. The three star graph ensembles in the Wigner-Dyson classes are defined by the d-vertex factors to be given now. We only give the d-vertex factors for in- and outgoing full lines. The corresponding factors for d-vertices connected to dashed lines is just the complex conjugate. In class AI each d-vertex carries a random phase factor

$$A\text{I}: \qquad \begin{array}{c}\big\uparrow\\ \bullet\,j\end{array} = e^{i\beta_j}. \qquad (9)$$

In class AI we have four different scattering processes corresponding to incoming and outgoing spin directions

$$A:\qquad \begin{aligned} \begin{array}{c}\uparrow\\ \bullet\,j\\ \uparrow\end{array} &= \frac{e^{i(\beta_j+\gamma_j)}}{\sqrt{2}} \qquad & \begin{array}{c}\uparrow\\ \bullet\,j\\ \downarrow\end{array} &= \frac{e^{i(\beta_j+\delta_j)}}{\sqrt{2}}\\[2mm] \begin{array}{c}\downarrow\\ \bullet\,j\\ \uparrow\end{array} &= \frac{e^{i(\beta_j-\delta_j)}}{\sqrt{2}} \qquad & \begin{array}{c}\downarrow\\ \bullet\,j\\ \downarrow\end{array} &= \frac{e^{i(\beta_j-\gamma_j)}}{\sqrt{2}}. \end{aligned} \qquad (10)$$

Thus spin either flips with probability $\frac{1}{2}$. In class AII iso-spin always flips at a d-vertex while spin flips with probability $\frac{1}{2}$. Thus there are altogether eight different processes

$$A\text{II}:\qquad \begin{aligned} \begin{array}{c}\uparrow\Uparrow\\ \bullet\,j\\ \uparrow\Downarrow\end{array} &= \begin{array}{c}\downarrow\Downarrow\\ \bullet\,j\\ \downarrow\Uparrow\end{array} = \frac{e^{i(\beta_j+\gamma_j)}}{\sqrt{2}}\\[2mm] \begin{array}{c}\uparrow\Uparrow\\ \bullet\,j\\ \downarrow\Downarrow\end{array} &= (-1)\times \begin{array}{c}\uparrow\Downarrow\\ \bullet\,j\\ \downarrow\Uparrow\end{array} = \frac{e^{i(\beta_j+\delta_j)}}{\sqrt{2}}\\[2mm] \begin{array}{c}\downarrow\Uparrow\\ \bullet\,j\\ \downarrow\Downarrow\end{array} &= \begin{array}{c}\uparrow\Downarrow\\ \bullet\,j\\ \uparrow\Uparrow\end{array} = \frac{e^{i(\beta_j-\gamma_j)}}{\sqrt{2}}\\[2mm] (-1)\times\begin{array}{c}\downarrow\Uparrow\\ \bullet\,j\\ \uparrow\Downarrow\end{array} &= \begin{array}{c}\downarrow\Downarrow\\ \bullet\,j\\ \uparrow\Uparrow\end{array} = \frac{e^{i(\beta_j-\delta_j)}}{\sqrt{2}}. \end{aligned} \qquad (11)$$

For the novel symmetry classes the wave function has either two (classes C and CI) or four components (D, DIII, AIII, BDI, and CII). In either case the components are divided in "electron" and "hole" components. Electrons are represented by full lines and holes by dashed lines. Additionally for the four-component wave functions, electrons (holes) have a "spin" up and down component. For each ensemble of star graphs the peripheral scattering involves complete electron-hole conversion (Andreev scattering). Thus, each d-vertex is connected to one dashed and one full line. For the graphs in the classes C and CI they are two different scattering processes at a d-vertex one for an incoming electron the other for an incoming hole. The corresponding d-vector factors are given by

$$C,\ C\text{I}: \qquad \overset{\uparrow}{\underset{\vdots}{\bullet}}{}_j\ =-\mathrm{e}^{-\mathrm{i}\beta_j} \qquad \overset{\vdots}{\underset{\uparrow}{\bullet}}{}_j\ =\mathrm{e}^{\mathrm{i}\beta_j} \qquad (12)$$

where $0 \le \beta_j < 2\pi$ is a random phase in class C and $\beta_j = 0$ or $\beta_j = \pi$ with equal probability in class CI. In the remaining classes spin flips with probability $\frac{1}{2}$ at each d-vertex. There are altogether eight scattering processes and their d-vertex factors are given by

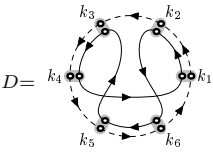|	D	DIII	AIII	BDI	CII
$\overset{\uparrow}{\underset{\uparrow}{\bullet}}_j$	$\dfrac{\mathrm{e}^{-\mathrm{i}\beta_j}}{\sqrt{2}}$	$\dfrac{\mathrm{e}^{-\mathrm{i}\beta_j}}{\sqrt{2}}$	$\dfrac{\tau_j}{\sqrt{2}}$	$\dfrac{\sigma_j}{\sqrt{2}}$	$\dfrac{-\sigma_j}{\sqrt{2}}$
$\overset{\uparrow}{\underset{\uparrow}{\bullet}}_j$	$\dfrac{-\mathrm{e}^{\mathrm{i}\gamma_j}}{\sqrt{2}}$	$\dfrac{-\mathrm{i}\sigma_j}{\sqrt{2}}$	$\dfrac{\mathrm{e}^{-\mathrm{i}\gamma_j}}{\sqrt{2}}$	$\dfrac{\mathrm{e}^{\mathrm{i}\beta_j}}{\sqrt{2}}$	$\dfrac{-\mathrm{e}^{-\mathrm{i}\beta_j}}{\sqrt{2}}$
$\overset{\uparrow}{\underset{\downarrow}{\bullet}}_j$	$\dfrac{\mathrm{e}^{-\mathrm{i}\gamma_j}}{\sqrt{2}}$	$\dfrac{-\mathrm{i}\sigma_j}{\sqrt{2}}$	$\dfrac{\mathrm{e}^{\mathrm{i}\gamma_j}}{\sqrt{2}}$	$\dfrac{\mathrm{e}^{-\mathrm{i}\beta_j}}{\sqrt{2}}$	$\dfrac{-\mathrm{e}^{\mathrm{i}\beta_j}}{\sqrt{2}}$
$\overset{\downarrow}{\underset{\downarrow}{\bullet}}_j$	$\dfrac{\mathrm{e}^{\mathrm{i}\beta_j}}{\sqrt{2}}$	$\dfrac{\mathrm{e}^{\mathrm{i}\beta_j}}{\sqrt{2}}$	$\dfrac{-\tau_j}{\sqrt{2}}$	$\dfrac{-\sigma_j}{\sqrt{2}}$	$\dfrac{\sigma_j}{\sqrt{2}}$
$\overset{\uparrow}{\underset{\uparrow}{\bullet}}_j$	$\dfrac{\mathrm{e}^{\mathrm{i}\beta_j}}{\sqrt{2}}$	$\dfrac{\mathrm{e}^{\mathrm{i}\beta_j}}{\sqrt{2}}$	$\dfrac{\sigma_j}{\sqrt{2}}$	$\dfrac{\sigma_j}{\sqrt{2}}$	$\dfrac{\sigma_j}{\sqrt{2}}$
$\overset{\downarrow}{\underset{\uparrow}{\bullet}}_j$	$\dfrac{-\mathrm{e}^{-\mathrm{i}\gamma_j}}{\sqrt{2}}$	$\dfrac{\mathrm{i}\sigma_j}{\sqrt{2}}$	$\dfrac{\mathrm{e}^{-\mathrm{i}\beta_j}}{\sqrt{2}}$	$\dfrac{\mathrm{e}^{-\mathrm{i}\beta_j}}{\sqrt{2}}$	$\dfrac{\mathrm{e}^{-\mathrm{i}\beta_j}}{\sqrt{2}}$
$\overset{\uparrow}{\underset{\downarrow}{\bullet}}_j$	$\dfrac{\mathrm{e}^{\mathrm{i}\gamma_j}}{\sqrt{2}}$	$\dfrac{\mathrm{i}\sigma_j}{\sqrt{2}}$	$\dfrac{\mathrm{e}^{\mathrm{i}\beta_j}}{\sqrt{2}}$	$\dfrac{\mathrm{e}^{\mathrm{i}\beta_j}}{\sqrt{2}}$	$\dfrac{\mathrm{e}^{\mathrm{i}\beta_j}}{\sqrt{2}}$
$\overset{\downarrow}{\underset{\downarrow}{\bullet}}_j$	$\dfrac{\mathrm{e}^{-\mathrm{i}\beta_j}}{\sqrt{2}}$	$\dfrac{\mathrm{e}^{-\mathrm{i}\beta_j}}{\sqrt{2}}$	$\dfrac{-\sigma_j}{\sqrt{2}}$	$\dfrac{-\sigma_j}{\sqrt{2}}$	$\dfrac{-\sigma_j}{\sqrt{2}}$

$$(13)$$

where $0 \le \gamma_j, \beta_j < 2\pi$ are random phases and $\sigma_j, \tau_j = \pm 1$ with equal probability.

C. Diagrammatic expansion of the ensemble averaged form factors

For the Wigner-Dyson classes we are only interested in the second-order form factor as the first-order form factor vanishes exactly under the ensemble average. For the graphs in the novel classes the ensemble average is non-trivial for the first-order form factor. The second-order form factor in the novel classes would contain additional contributions proportional to $\langle s_n^2 \rangle$ and its complex conjugate which vanish in the Wigner-Dyson case. We will not consider the second-order form factor for other classes than the Wigner-Dyson here.

Though the second-order form factor is a sum over pairs of periodic orbits and the first-order form-factor contains a single orbit the diagrammatic expansion is based on similar observations. We will start with the Wigner-Dyson case. Most pairs of periodic orbits do not survive the ensemble average. A contribution can only survive if all d-vertices have a partner d-vertex such that the product of their factors does not depend on the random phases or random signs. In the This condition can only be fulfilled if the two orbits visit the same peripheral vertices with the same multiplicities. The order may however be different and one may introduce diagrams to denote the various appearing permutations. Let us start with the diagrams for class AI and later introduce the spin degrees of freedom. An example of such a diagram for $n = 6$ is given by

$$D= \quad \text{}$$

$$=\xi \sum_{k_1,\ldots,k_6=1}^{B} \frac{\mathrm{e}^{\frac{2\pi\mathrm{i}}{B}\sum_{m=1}^{6}(k_{\tilde{\pi}(m)}k_{\tilde{\pi}(m+1)}-k_m k_{m+1})}}{B^6}=\frac{\xi}{B^2}. \qquad (14)$$

In this diagram d-vertices have been joined to pairs in a grey area to indicate that they carry the same index k_m. We will call these grey areas *scattering regions* and, in the sequel, we will drop the indices k_m (as well as line indices for multi-component wave functions). The *multiplicity factor* ξ will be explained later in this section.

Any diagram that contributes to $K_{2,n}$ has $2n$ d-vertices connected by $2n$ (directed) lines that define two periodic orbits of length n. One of the orbits has only full lines the other only dashed lines. Each d-vertex and each line contributes with the corresponding factor to the diagram – since by construction the phase factors $\mathrm{e}^{\mathrm{i}\beta_j}$ each have a partner $\mathrm{e}^{-\mathrm{i}\beta_j}$ the phases all cancel. The number w of scattering regions may range in $w = n, n-1, \ldots, 1$. Each of the w scattering regions carries a single index k_m ($m = 1, 2, \ldots, w$) for all d-vertices which it contains. The number of d-vertices in a scattering region is always even – half of the d-vertices are part of each of the two periodic orbits. If $w < n$ we will call the diagram a *sub-diagram* – in sub-diagrams some g-vertices contain more

than two d-vertices.

In the classes A and AII each line gets an additional index α_j ($j = 1, 2, \ldots, 2n$) for the different (spin and iso-spin) components of the wave function. The sum over α_j collapses to a sum over allowed component configurations when under the averages over δ_j and γ_j. An allowed component configuration is a set of line indices α_j for which all phases δ_j and γ_j along the diagram cancel exactly. Then the product of all phase factors is ± 1. The sum over the w indices k_m for the different encounter regions and the sum over allowed component configurations factorizes such that the value of a diagram D_ν falls into three parts

$$D_\nu = \xi_\nu C_\nu P_\nu. \tag{15}$$

Here, $\xi_n u$ is the multiplicity factor that, C_ν is the *quasi-spin* factor, and P_ν the *principal part*. The latter contains only the line factors $\frac{1}{\sqrt{B}} e^{\pm i \frac{2\pi}{B} k_m k_{m'}}$ and is summed over the w scattering region indices k_m. The quasi-spin factor C_ν contains all the d-vertex factors which are summed over all allowed quasi-spin (component) configurations – in class AI one has $C_\nu = 1$ in the classes A and AII it is given by $\pm \frac{1}{2^n}$ for each allowed configuration. In class A the sign is always positive, so C_ν is $\frac{1}{2^n}$ times the number of allowed configurations. In class AII quasi-spin configurations a negative sign appears if an allowed configuration contains an odd number of d-vertices where the incoming spins and iso-spins are anti-parallel and both flip (see (11)).

Finally, the multiplicity factor $\xi_\nu = \frac{\tilde\xi}{n}$ is the number $\tilde\xi$ of times the diagram appears as a sub-sum in the original form factor (7) before the average was performed divided by the length of the orbit n. In general the sum over the indices k_m is a sum over pairs of points on two different periodic orbits. However, any pair of two points along the same orbits will give exactly the same contribution. Thus, in general the sum over k_m appears $\tilde\xi = n^2$ times in the original one – in the diagram (14) one has indeed $\tilde\xi = n^2 = 36$ times. There are exceptions whenever one orbit is a repetition of a shorter orbit or if the diagram is invariant with respect to some cyclic permutation of the indices k_m. For example the diagrams

$$D_1^{(0)} = \quad \text{and} \quad D_2^{(0)} = \tag{16}$$

only appear n times in the original sum such that $\tilde\xi = n$ and $\xi_1^{(0)} = \xi_2^{(0)} = 1$. These are the two diagrams of the diagonal approximation to be discussed in the next section.

Obviously every pair of periodic orbits visiting the same scattering regions defines a diagram. However, if one sums over all the scattering region indices k_m without restriction the same pair of periodic orbits may appear in different diagrams and we have to face the problem of double (or multiple) counting of periodic orbits. One way to get rid of the double counting problem is to restrict the sum over k_m such that $k_i \neq k_j$ for $i \neq j$ and add all sub-diagrams where the number w of scattering regions is smaller than n (with the same restriction in the sum over indices). The form factor $K_{2,n}$ can then be written as a sum over all diagrams with $w = n, n-1, \ldots, 1$ scattering regions and every pair of periodic orbits is counted exactly once.

It will be more convenient for us to keep an unrestricted sum over the scattering regions and subtract the multiply counted counted orbits. Any diagram D contains many sub-diagrams which can be obtained from D by combining some scattering regions to a single one. This is equivalent to restricting the sum in the diagram to $k_i = k_j$. Multiple counting occurs when either two (or more) diagrams D_1 and D_2 have the same sub-diagram or when one sub-diagram appears more than once in the same diagram D. If the wave function has one component we just have to subtract the overcounted sub-diagrams. In the presence more than one component only the over-counted quasi-spin configurations have to subtracted. It may happen that a sub-diagram allows new quasi-spin configurations that have not been counted in the original diagram – then the corresponding configurations have to be added. Luckily we will not encounter such difficulties in the sequel.

Finally, we may write the second-order form factor as a sum over diagrams

$$K_{2,n} = \frac{1}{g\mu B}\langle |s_n|^2 \rangle = \frac{n}{g\mu B}\left(\sum_\nu D_\nu - \sum_{\nu'} D_{\nu'}^{\text{sub}} \right). \tag{17}$$

The sum over diagrams D_ν only contains diagrams with $w = n$ scattering regions. The sum over sub-diagrams $D_{\nu'}^{\text{sub}}$ accounts for the corrections due to multiple counting – it contains diagrams with $w = n-1, n-2, \ldots, 1$ scattering regions and we include the number of times it has been overcounted in the multiplicity factor. Note, the factor n outside the parentheses – this factor appears due to the definition of the multiplicity factor ξ.

The diagrammatic representation of the first-order form factor in the novel symmetry classes is analogous. The main difference is that there is only a single periodic orbit connecting n d-vertices any diagram that contributes to $K_{1,n}$. Due to complete Andreev scattering at the peripheral vertices. As a consequence the d-vertices in the diagrams always connect a full line with a dashed line. Diagrams can thus only be drawn if the length n of the orbit is even and

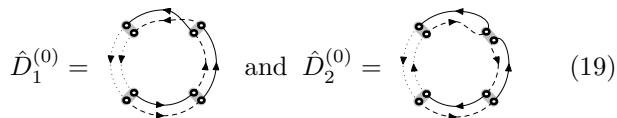$$s_n = 0 \qquad \text{if } n \text{ is odd}. \tag{18}$$

Similar as before for the second-order form factor most contributions to the trace s_n do not survive the average over the phases γ_j, β_j (and signs σ_j, τ_j). The non-vanishing contributions can again be grouped in diagrams where at most $\frac{n}{2}$ d-vertex indices remain independent. In

a non-vanishing diagram each d-vertex has again a partner such that the product of their d-vertex factors does not depend on the random phase factors or signs. We again introduce *Scattering regions* that are defined as in the diagrams to the second-order form factor. Each scattering region has a single index which is the same for all d-vertices it contains. A scattering region always contains an even number of d-vertices.

A general diagram will be drawn without indices and has a value $\hat{D}_\nu = \hat{\xi}_\nu \hat{C}_\nu \hat{P}_\nu$ where the definitions of the principal part $\hat{P}_\nu$ and the quasi-spin factor $\hat{C}_\nu$ are as before. The hat serves as a symbol to distinguish between the contributions to the first-order form factor (with hat) form those to the second-order form factor (no hat). The principal part is independent of the symmetry group and given by the line contributions summed over the indices of the scattering regions.

The quasi-spin factor $\hat{C}_\nu$ is the sum of the d-vertex factors over allowed spin and electron-hole configurations. The quasi-spin factor may also vanish. If there is no spin it will be ± 2 where the factor 2 is due to interchanging all electron and hole lines.

The multiplicity factor $\hat{\xi}$ is here defined as the number of times an equivalent sum appears in the original sum s_n – note, that here we have not divided this number by n as in the case of the diagrams for the second-order form factor. As an example the two diagrams

$$\hat{D}_1^{(0)} = \quad \text{and} \quad \hat{D}_2^{(0)} = \qquad (19)$$

have multiplicity factors $\hat{\xi}_1^{(0)} = 1$ and $\hat{\xi}_2^{(0)} = \frac{n}{2}$. The difference is due to the different symmetry in the two diagrams. For the second diagram the rotational symmetry is broken by the turning point of the periodic orbit. These two diagrams correspond to the self-dual approximation to be discussed in the next section.

Multiple countings have to be accounted for in the same manner as for the second-order form factor which results in

$$K_{1,n} = \frac{2}{g}\langle s_n \rangle = \frac{2}{g}\left(\sum_\nu D_\nu - \sum_{\nu'} D_{\nu'}^{\text{sub}} \right) \qquad (20)$$

by including the corresponding sub-diagrams. For finite n the sum over diagrams is finite for both types of form factors and the expansion converges absolutely. As every periodic orbit (pair of period orbits) defines some diagram no contribution is neglected and the expansion is formally exact.

III. THE DIAGONAL AND SELF-DUAL APPROXIMATIONS AND BEYOND

While the calculation of the principal part, quasi-spin factor and multiplicity factor for any given diagram is quite simple, the sum over all diagrams defined in the previous section is quite non-trivial. We will now give a systematic short-time expansion of this sum in the ergodic limit $B \to \infty$. In the leading order only two diagrams have to be accounted for in each symmetry class. More diagrams have to be taken into account for the next to leading order where multiple-counting of periodic orbits lead to additional complexity.

A. The diagrammatic short-time expansion of the form factors

We will be interested in the short-time behavior of large graphs such that we may assume $1 \ll n \ll \frac{\mu B}{g}$. The first inequality $1 \ll n$ assures that we are in the universal regime – the ultra-short-time behavior where $n = \mathcal{O}(1)$ is known to be dominated by the system-dependent shortest orbits. The second inequality can be rewritten as $\tau \equiv \frac{gn}{\mu B} \ll 1$ which shows that we are interested in times much shorter than Heisenberg time.

We want to calculate $K_{1,n}$ and $K_{2,n}$ in the limit $n, B \to \infty$ where $\tau = \frac{gn}{\mu B} \ll 1$ is constant. For that aim we will expand the form factors in orders of τ:

$$K_1\left(\tau = \frac{gn}{\mu B}\right) = \overline{\frac{2}{g}\langle s_n \rangle} = \frac{2}{g}\sum_{m=0}^\infty \mathcal{K}_1^{(m)} \qquad (21)$$

$$K_2\left(\tau = \frac{gn}{\mu B}\right) = \overline{\frac{1}{g\mu B}\langle |s_n|^2 \rangle} = \frac{\tau}{g^2}\sum_{m=0}^\infty \mathcal{K}_2^{(m)} \qquad (22)$$

where $\mathcal{K}_{1,2}^{(m)}$ are expansion coefficients proportional to τ^m that we have to calculate – in this expansion we have anticipated that the leading order will be a constant for $K_1(\tau)$ and will be linear in $K_2(\tau)$.

Each of these coefficients is a time averaged sum over some diagrams (and sub-diagrams). The time average is performed over a short discrete time interval $[n, n + \Delta n]$ and has to be performed before we take the limit $n, B \to \infty$. The interval has to chosen such that $\Delta\tau = \frac{g\Delta n}{\mu B}$ vanishes in that limit.

Let us shortly summarize the procedure: *i.* find all diagrams and sub-diagrams that contribute to a given order $\mathcal{K}_{1,2}^{(m)}$ for finite $B \gg n \gg 1$, *ii.* for every sub-diagram with w vertices count how often it appears as a sub-diagram of other (sub)diagrams in the same order $\mathcal{K}_{1,2}^{(m)}$ *and* in all smaller orders $\mathcal{K}_{1,2}^{(m-1)}, \ldots$, *iii.* calculate the values of the diagrams and add them and subtract the overcounted sub-diagrams, *iv.* take the time average over n, *vi* finally take the limit $n, B \to \infty$. Obviously the procedure is recursive and one has to start with $m = 0$.

The rest of this section will be devoted to the description of the diagrams that contribute to a given order $\mathcal{K}_{1,2}^{(m)}$. Since $\tau = \frac{gn}{\mu B}$ this is equivalent to finding the diagrams with values of order B^{-m}. A single diagram which is of order B^{-m} in B may have a very different order in n – such that the limit $n, B \to \infty$ cannot always

be performed for a single diagram. Our procedure will be self-consistent if this limit exists *after* we have summed over all (sub)diagrams.

As the multiplicity factor and the quasi-spin factor do not depend on B we have to look at the principal part which does not depend on the symmetry class. The resulting expansion for the first-order form factor can used for all graphs in the novel symmetry classes while the diagrams in the expansion of the second-order form factor are the same for all three Wigner-Dyson graphs. The difference between the ensembles is mainly due to different quasi-spin factors. Note, that these may vanish.

The principal par of a (sub)diagram D_ν for $\mathcal{K}_2^{(m)}$ ($\hat{D}_\nu$ for $\mathcal{K}_1^{(m)}$) with $2n$ (n) d-vertices and lines and $w \leq n$ ($w \leq \frac{n}{2}$) different scattering regions is bounded from above

$$P_\nu \leq \frac{1}{B^{n-w}} \qquad \hat{P}_\nu \leq \frac{1}{B^{\frac{n}{2}-w}} \ . \qquad (23)$$

Indeed, the absolute value of the summand in the principal part is $\frac{1}{B^n}$ ($\frac{1}{B^{\frac{n}{2}}}$) stemming from the $2n$ (n) amplitudes of the line contributions when one sums over w indices $k_m = 1, 2, \ldots, B$. In (23) equality holds if all the phases acquired along the lines cancel exactly. This is the case in *complete* (sub)diagrams for which every full line that connects two scattering regions is accompanied by a dashed line connecting the same two scattering regions. We will call such a pair of lines a *complete diagonal (anti-diagonal)* pair of lines if they start and end at the same (opposite) scattering region.

Every complete (sub)diagram with $w = n - m$ ($w = \frac{n}{2} - m$) scattering regions contributes as a (sub)diagram to $\mathcal{K}_2^{(m)}$ ($\mathcal{K}_1^{(m)}$). If $w < n - m$ ($w < \frac{n}{2} - m$) no sub-diagrams exist that contribute.

It remains to find the non-complete (sub)diagrams. For non-complete diagrams the sum is oscillating due to the appearing phase factors. An oscillating sum over one index is of the form

$$\sum_{k=1}^{B} e^{\frac{2\pi i}{B} k(k'-k'')} = B\delta_{k'k''} \qquad (24)$$

where $\delta_{k'k''}$ is the Kronecker symbol. The subsequent sum over k' does not give an additional factor B. Thus non-complete (sub)diagrams can only contribute to $\mathcal{K}_2^{(m)}$ ($\mathcal{K}_1^{(m)}$) if they have a complete sub-diagram with $w = n - m$ scattering regions.

All (sub)diagrams for $\mathcal{K}_2^{(m)}$ ($\mathcal{K}_1^{(m)}$) are thus found by first finding all complete (sub)diagrams with $n - m$ ($\frac{n}{2} - m$) scattering regions and then finding all (non-complete) diagrams with $n - m + 1, \ldots, n$ ($\frac{n}{2} - m + 1, \ldots, \frac{n}{2}$) scattering regions which contain one of the complete sub-diagrams.

B. The diagonal approximation and beyond for star graphs in the Wigner-Dyson classes

We will now find all diagrams that contribute to the diagonal approximation ($m = 0$) and one order beyond in the second-order form factor of star graphs in the Wigner-Dyson classes. The coefficients $\mathcal{K}_2^{(0)}$ and $\mathcal{K}_2^{(1)}$ will be calculated. The resulting form factors will be in accordance with the random-matrix predictions [16] (for $\tau \ll 1$)

$$K_2(\tau) = \begin{cases} \tau & \text{GUE } (A\text{-GE}) \\ 2\tau - 2\tau^2 + \mathcal{O}(\tau^3) & \text{GOE } (A\text{I-GE}) \\ \frac{\tau}{2} + \frac{\tau^2}{4} + \mathcal{O}(\tau^3) & \text{GSE } (A\text{Ii-GE}). \end{cases} \qquad (25)$$

1. The diagrams

For the diagonal approximation ($m = 0$) – we just have to find all complete diagrams with two periodic orbits of length n and $w = n$ scattering regions. There are two such diagrams: $D_1^{(0)}$ and $D_2^{(0)}$ given by (16). In $D_1^{(0)}$ the two periodic orbits are the same and in $D_2^{(0)}$ one orbit is the time-reversed orbit of the other. We have

$$\mathcal{K}_2^{(0)} = \overline{D_1^{(0)} + D_2^{(0)}} \qquad (26)$$

which gives the diagonal approximation. The multiplicities of the two diagrams are $\xi_1^{(0)} = \xi_1^{(0)} = 1$ and their principal parts $P_1^{(0)} = P_2^{(0)} = 1$. Only the quasi-spin contributions depend on the symmetry class such that

$$D_1^{(0)} = C_1^{(0)} \qquad \text{and} \qquad D_2^{(0)} = C_2^{(0)} \qquad (27)$$

We will see in section III B 2 that for broken time-reversal the quasi-spin contribution of the diagram $D_2^{(0)}$ vanishes in the limit $n \to \infty$.

For the first order beyond the diagonal approximation ($m = 1$) we have to find all complete sub-diagrams with $n-1$ scattering regions and then all new non-complete diagrams with n scattering regions that contain one of the complete sub-diagrams. The diagrams can be grouped into three families. Each of the families contains complete and non-complete diagrams. The complete diagrams of the first two families appear trivially as a sub-diagram of the diagonal diagrams $D_1^{(0)}$ and $D_2^{(0)}$ by joining two of their scattering regions

$$D_{1,l}^{\text{sub},(1)} = \quad \text{} \quad = C_{1,l}^{\text{sub},(1)} \frac{n}{B} \quad (28\text{a})$$

$$D_{2,l}^{\text{sub},(1)} = \quad \text{} \quad = C_{2,l}^{\text{sub},(1)} \frac{n}{B} \quad (28\text{b})$$

where we have already included the principal part $P = \frac{1}{B}$ and the multiplicity $\xi = n$. The integer $l = 0, 1, \ldots, n-2$ gives the number of scattering regions in the left loop (the central scattering region is not counted). The diagram with l vertices in the left loop is equivalent to the one with l vertices in the right loop. The non-complete diagrams of the first two families each contain one of corresponding complete sub-diagrams

$$D_{1,l}^{(1)} = \qquad = \qquad C_{1,l}^{(1)} \frac{n}{B} \quad (29a)$$

$$D_{2,l}^{(1)} = \qquad = \qquad C_{2,l}^{(1)} \frac{n}{B}. \quad (29b)$$

Again, $l = 0, 1, \ldots$ is the number of scattering regions in the left loop (the two central scattering regions are not counted). Let us now assume that the quasi-spin factors within one family of diagrams is the same $C_{1,l}^{(1)} = C_{1,l}^{\text{sub},(1)} \equiv C_1^{(1)}$ and $C_{1,l}^{(1)} = C_{2,l}^{\text{sub},(1)} \equiv C_2^{(1)}$. In the limit $n, B \to \infty$ this can indeed be shown for each of the symmetry classes. The contribution of these two families then vanishes due to overcounting. Each of the sub-diagrams has been counted once in the diagonal approximation and is also a sub-diagram of the new non-complete diagrams.

The third family contains all non-trivial diagrams that correspond to the Sieber-Richer pairs. They consist of two loops as well, however in one loop the two orbits are parallel while in the other they are time-reversed

$$D_{3,l}^{\text{sub},(1)} = \qquad = C_{3,l}^{\text{sub},(1)} \frac{n}{B}. \quad (30)$$

In these diagram it is irrelevant if we draw the crossing on the left or on the right of the central scattering region. If the left or the right loop has either zero or one vertex it is indistinguishable from one of the corresponding previous diagrams (28a) or (28b). Thus $l = 2, 3, \ldots, n-4$ and there are $n-5$ new diagrams of this form. Note, that these diagrams are *not* sub-diagrams of the diagonal diagrams $D_1^{(0)}$ and $D_2^{(0)}$.

The corresponding non-complete diagrams diagrams are

$$D_{3,l}^{(1)} = \qquad = C_{3,l}^{(1)} \frac{n}{B}. \quad (31)$$

The number of vertices in the left loop (left of the crossing) runs from $l = 4$ to $l = n-4$ – all other diagrams are indistinguishable from corresponding diagrams in the

families (29a) or (45b). Thus there are $n-7$ new diagrams in this family.

Each of the sub-diagrams $D_{3,l}^{\text{sub},(1)}$ is contained once in the diagrams $D_{3,l}^{(1)}$ and $D_{3,l+2}^{(1)}$ if $4 \leq l \leq n-6$ while for $l = 2, 3$ ($l = n-4, n-5$) they are contained once in one $D_{2,l}^{(1)}$ and $D_{3,l+2}^{(1)}$ ($D_{1,l+2}^{(1)}$ and $D_{3,l}^{(1)}$). Thus each sub-diagrams $D_{3,l}^{\text{sub},(1)}$ has been overcounted once. Again one can show that $C_{3,l}^{(1)} = C_{3,l}^{\text{sub},(1)} \equiv C_3^{(1)}$ in the limit $n, B \to \infty$. The contributions does then not vanish if $C_3^{(1)} \neq 0$ and one has

$$K_2^{(1)} = -2\overline{C_3^{(1)}}. \quad (32)$$

2. Wigner-Dyson class AI (GOE)

Since the graphs in symmetry class AI have a one-component wave function ($\mu = g = 1$) the quasi-spin contribution to any (sub)diagram D_ν is $C_\nu = 1$. In the diagonal approximation each the two diagrams has the value $D_1^{(0)} = D_2^{(0)} = 1$ and we have

$$\mathcal{K}_2^{(0)} = 2. \quad (33)$$

For the next order we have $D_{3,l}^{(1)} = D^{\text{sub},(1)} = \tau$ which gives

$$\mathcal{K}_2^{(1)} = -2\tau. \quad (34)$$

Altogether the leading terms of the second-order form factor give $K_2(\tau) = 2\tau - 2\tau^2 + \mathcal{O}(\tau^3)$ in accordance with the GOE prediction (25).

3. Wigner-Dyson class A (GUE)

In class A we have defined star graphs with a two-component wave function ($\mu = 2$, $g = 1$) and we have to calculate the quasi-spin contributions for all diagrams.

Let us start with diagram $D_1^{(0)}$ where both periodic orbits are the same (parallel). Only spin configurations survive the average over the phases γ_k and δ_k for which the spins on two parallel lines is the same. The spins on lines that connect different scattering regions are independent. Thus there are 2^n allowed spin configurations and the quasi-spin contribution to the diagram is $C_1^{(0)} = 1$ which results in

$$D_1^{(0)} = 1. \quad (35)$$

In the diagram $D_2^{(0)}$ the two orbits are anti-parallel. Here, the spins on different lines are not independent for configurations that survive the phase average. If at any pair of anti-parallel lines the two spins are σ_1 for the full line and σ_2 for the dashed line the spins on the neighboring lines are σ_1 for the dashed line and σ_2 for

the full line. If n is even σ_1 and $sigma_2$ are independent while for odd n they are equal. So there are only four (two) allowed spin configurations for even (odd) n which gives

$$D_2^{(0)} = \frac{3 + (-1)^n}{2^n}. \qquad (36)$$

This value is exponentially suppressed in the limit $n \to \infty$ – a consequence of breaking the time-reversal invariance in this symmetry class.

In the first order beyond the diagonal approximation the contribution of the first family vanishes because the quasi-spin factor is the same throughout the family (see section III B 1). The contribution of the second family vanishes because their quasi-spin factor all vanish in the limit $n, B \to \infty$. For the third family the quasi-spin factors are not equal for each diagram in the group. Its value is small if it contains a big anti-parallel loop. There are however diagrams with a short anti-parallel loop. It is however not difficult to calculate the quasi-spin factor of each diagram which gives

$$\begin{aligned} D_{3,l}^{(1)} &= \frac{3-(-1)^{n-l}}{2^{n-l-1}} \frac{n}{B} \\ D_{3,l}^{\mathrm{sub},(1)} &= \frac{3-(-1)^{n-l}}{2^{n-l-1}} \frac{n}{B} \end{aligned} \qquad (37)$$

The sum over all these contributions (including the correct accounting for multiple counting) is

$$\sum_{l=4}^{n-4} D_{3,l}^{(1)} - \sum_{l=2}^{n-4} D_{3,l}^{\mathrm{sub},(1)} = -D_{3,2}^{\mathrm{sub},(1)} - D_{3,3}^{\mathrm{sub},(1)} = -\frac{9+(-1)^n}{2^{n-3}} \frac{n}{B} \qquad (38)$$

which also vanishes in the limit $n \to \infty$. Thus Sieber-Richter pairs do not contribute for broken time-reversal symmetry.

Only the diagrams of the diagonal approximation contribute to the form factor which has the value $K_2(\tau) = \tau$ as predicted by the GUE (25) for $\tau < 1$.

4. Wigner-Dyson class AII (GSE)

In class AII we have a four-component wave function on the star graphs ($\mu = 4$, $g = 2$). At each d-vertex iso-spin flips while spin may either flip or not. As an immediate consequence the length of every periodic orbit is even and $s_n = 0$ if n is odd.

For the diagonal approximation we have to recalculate the quasi-spin factors of the two diagrams $D_1^{(0)}$ and $D_2^{(0)}$ with the additional spin and iso-spin freedoms. Let us start with the first diagram where both orbits traverse the scattering regions in the same order. The iso-spins on parallel lines are either always parallel or always anti-parallel. If iso-spins on parallel lines are parallel only the spin configurations which are everywhere parallel as well survive the average. As the spins on lines connecting different scattering regions are independent there are 2^{n+1} such configurations with parallel iso-spins (n factors 2 from the spins and one factor from the iso-spin).

If the iso-spins are all anti-parallel there are allowed configurations with either all spins parallel or all anti-parallel between two scattering regions. If the spins are all anti-parallel they never flip and if they are parallel they both flip at every scattering region. Altogether there are only 8 configurations with anti-parallel iso-spins which implies that these contributions are negligible in the limit $n, B \to \infty$. Note, that anti-parallel iso-spins implies that the two orbits are different and not related by time-reversal. At each d-vertex with an incoming spin that is antiparallel to the incoming iso-spin a factor -1 is gathered if the spin flips. All factors -1 within one scattering region cancel because the two d-vertices have the same configuration.

Due to time-reversal invariance the two diagrams in the diagonal approximation have the same value

$$D_1^{(0)} = D_2^{(0)} = 2 + 2^{-n+3}. \qquad (39)$$

Note, that time-reversal implies changing the directions of arrows flipping the spins while iso-spins do not flip. In the time-reversed diagram $D_2^{(0)}$ the factors -1 cancel in a slightly different way. As on neighboring lines spins are always anti-parallel and iso-spins always parallel one gets a factor -1 at every scattering region where both spins flip. Since n is even so is the number of spin flips along each orbit.

For the calculations of the diagrams that contribute beyond the diagonal approximation we will neglect all contributions that are exponentially suppressed. The first two families have a vanishing contribution as their quasi-spin factors are the same within each family in the limit $n, B \to \infty$. Again, we only have to consider the Sieber-Richter family with the diagrams $D_{3,l}^{(1)}$ and $D_{3,l}^{\mathrm{sub},(1)}$. In both families only even l can give contributions that are not exponentially suppressed as iso spins have to remain parallel in the left and right loops. There are $\frac{n}{2} - 3$ contributing diagrams in the family $D_{3,l}^{(1)}$ and $\frac{n}{2} - 2$ in the family $D_{3,l}^{\mathrm{sub},(1)}$ (each of them has been overcounted once). They all have the same value

$$D_{3,l}^{(1)} = D_{3,l}^{\mathrm{sub},(1)} = -\frac{n}{B}. \qquad (40)$$

For any quasi-spin configuration an odd number of factors -1 is gathered along the orbits – also the spins on the lines that connect the left and right loops are not independent.

Altogether we get

$$K_{2,n} = \frac{n}{8B} \begin{cases} 0 & \text{if } n \text{ odd,} \\ 4 + \frac{n}{B} + \mathcal{O}(\frac{n^2}{B^2}) & \text{if } n \text{ is even.} \end{cases} \qquad (41)$$

As $\tau = \frac{n}{2B}$ the time average yields $K_2(\tau) = \frac{\tau}{2} + \frac{\tau^2}{4} + \mathcal{O}(\tau^2)$ in accordance with the short-time expansion of the universal result (25) from the GSE .

C. The self-dual approximation and beyond for chiral and Andreev graphs

Now we will consider the self-dual approximation ($m = 0$) and one order beyond ($m = 1$) for the first-order form factors in the novel symmetry classes. We will give all diagrams and show that they add up to the corresponding random-matrix predictions [16] for $\tau \ll 1$

$$
K_1(\tau) = \begin{cases}
-1 & C\text{-GE} \\
-1 + \frac{\tau}{2} + \mathcal{O}(\tau^2) & C\text{I-GE} \\
1 & D\text{-GE} \\
\frac{1}{2} - \frac{\tau}{8} + \mathcal{O}(\tau^2) & D\text{III-GE} \\
-\frac{\tau}{2} + \mathcal{O}(\tau^2) & \text{chGUE}(A\text{III-GE}) \\
1 - \frac{3\tau}{2} + \mathcal{O}(\tau^2) & \text{chGOE}(BD\text{I-GE}) \\
-\frac{1}{2} - \frac{3\tau}{8} + \mathcal{O}(\tau^2) & \text{chGSE}(C\text{II-GE}).
\end{cases}
\tag{42}
$$

1. The diagrams

The self-dual approximation takes into account all complete diagrams for $K_{1,n}$ (where n is even) with $n/2$ scattering regions. The approximation has been called self-dual because the diagrams contain those orbits which are invariant under either a chiral symmetry or charge conjugation (in combination with time-reversal).

There are two self-dual diagrams which have been given in (19) where their multiplicity factors have been given. Their principal part is $\hat{P}_{1,2}^{(0)} = 1$. In the first diagram the same scattering regions are visited twice in the same order but with electrons replaced by holes in the second traversal. It vanishes exactly if $\frac{n}{2}$ is even (no complete diagram can then be drawn) while

$$
\hat{D}_1^{(0)} = \hat{C}_1^{(0)}, \tag{43}
$$

for odd $\frac{n}{2}$. In the second diagram the same orbits are traversed in opposite (time-reversed) direction. It contains one scattering region where the direction is changed. Its value is

$$
\hat{D}_2^{(0)} = \frac{n}{2}\hat{C}_2^{(0)}. \tag{44}
$$

If $n/2$ is odd the turning point region has one incoming electron and one incoming hole as drawn in (19). The diagram has to be changed slightly for even $n/2$ – then the turning point region has either two incoming electrons or two incoming holes.

To calculate the linear order of the form factor we need all families of diagrams that contribute to $\mathcal{K}_1^{(1)}$. Most of these diagrams will have a multiplicity factor $\hat{\xi} = \frac{n}{2}$ because there is no symmetry. The exceptions have $\hat{\xi} = \frac{n}{4}$ due to some two-fold symmetry. When we explicitly give the value of a family of diagrams they always refer to the generic case where no two-fold symmetry is present. The cumbersome accounting for all these cases will only be

done for those families of diagrams that do not vanish for different reasons.

The diagrams have either $n/2$ scattering regions, are not complete or they have $n/2 - 1$ scattering regions, are complete. In all cases the principal value is $\hat{P}_\nu^{(1)} = \frac{1}{B}$. One may group the diagrams into seven different families.

The first two families have complete diagrams that are sub-diagrams of the self-dual approximation. Joining two scattering regions in the two diagrams (19) gives

$$
\hat{D}_{1,l}^{\text{sub},(1)} = \quad\quad\quad\quad = \quad \hat{C}_{1,l}^{\text{sub},(1)} \frac{n}{2B} \quad (45a)
$$

$$
\hat{D}_{2,l,k}^{\text{sub},(1)} = \quad\quad\quad\quad = \quad \hat{C}_{2,l,k}^{\text{sub},(1)} \frac{n}{2B}. \quad (45b)
$$

where l is the number of scattering regions in the right loop. The first type of diagrams only exists if $\frac{n}{2}$ is odd. For the second type of diagrams k is an index for the different positions of the turning point.

There are two types of non-complete diagrams in each of the two families. For the first family they are given by

$$
\hat{D}_{1a,l}^{(1)} = \quad\quad\quad\quad = \frac{n}{2B}\hat{C}_{1a,l}^{(1)}
$$

$$
\hat{D}_{1b,l}^{(1)} = \quad\quad\quad\quad = \frac{n}{2B}\hat{C}_{1b,l}^{(1)}.
\tag{46}
$$

The difference between the two diagrams is that two central scattering regions have two incoming lines of the same type for the first diagram and two different incoming lines in the second. Both diagrams only exist for odd $\frac{n}{2}$.

For the second family one has

$$
\hat{D}_{2a,l,k}^{(1)} = \quad\quad\quad\quad = \frac{n}{2B}\hat{C}_{2a,l,k}^{(1)}
$$

$$
\hat{D}_{2b,l,k}^{(1)} = \quad\quad\quad\quad = \frac{n}{2B}\hat{C}_{2b,l,k}^{(1)}
\tag{47}
$$

which differ in the direction of the lower line. Both diagrams have been drawn for an even number $\frac{n}{2} - l - 2$ of scattering regions in the left loop. Then the two central scattering regions have one incoming dashed and one incoming full line each. For an odd number of scattering

regions in the left loop the central scattering regions have two incoming lines of the same type.

Each of the sub-diagrams $D_{1,l}^{\mathrm{sub},(1)}$ or $D_{2,l,k}^{\mathrm{sub},(1)}$ has been counted three times. Once ion the self-dual approximation and twice in the diagrams $D_{1a/1b,l,k}^{(1)}$ and $D_{2a/2b,l,k}^{(1)}$. If the quasi-spin factors do not differ in the limit $n, B \to \infty$ the diagrams cancel due to overcounting. This is indeed the case for all seven ensembles of star graphs in the novel symmetry classes.

The third family contains diagrams with two parallel complete loops. The complete diagrams in this family

$$\hat{D}_{3,l}^{\mathrm{sub},(1)} = \quad \begin{array}{c}\text{[diagram: } \tfrac{n}{2}-2-l \text{ , } l\text{]}\end{array} \quad . = \frac{n}{2B}\hat{C}_{3,l}^{\mathrm{sub},(1)} \quad (48)$$

cannot be obtained as sub-diagrams of the self-dual diagrams. In the second traversal of each loop the roles of electrons and holes are interchanged. A complete diagram can only be achieved if both $l = 0, 2, \dots$ and $\frac{n}{2} - l - 2 = 0, 2, \dots$ are even. Thus $\frac{n}{2}$ is even. The non-complete diagrams in this family are given by

$$\hat{D}_{3a,l}^{(1)} = \quad \begin{array}{c}\text{[diagram: } \tfrac{n}{2}-l \text{ , } l\text{]}\end{array} \quad = \frac{n}{2B}\hat{C}_{3a,l}^{(1)}$$

$$\hat{D}_{3b,l}^{(1)} = \quad \begin{array}{c}\text{[diagram: } \tfrac{n}{2}-2-l \text{ , } l\text{]}\end{array} \quad = \frac{n}{2B}\hat{C}_{3b,l}^{(1)}.$$

$$(49)$$

In both cases $\frac{n}{2}$ is even while and l is odd in the first type and even in the second type. If all quasi-spin factors within this family are equal the contribution of this family vanishes due to overcounting. Indeed for fixed even l the complete sub-diagrams $D_{3,l}^{\mathrm{sub},(1)}$ has been counted three times. It appears once in $D_{3b,l}^{(1)}$ and twice in the diagram $D_{3a,l+1}^{(1)}$ because there are two ways of joining diagonally opposite scattering regions. As the values of all diagrams are equal and the complete sub-diagram has been overcounted twice for each fixed even l the contributions cancel.

By introducing turning points in both loops or just in the right loop of the third family one arrives at the fourth and fifth family of diagrams. The complete diagrams in the fourth family are given by

$$\hat{D}_{4,l,k_l,k_r}^{\mathrm{sub},(1)} = \quad \begin{array}{c}\text{[diagram: } \tfrac{n}{2}-2-l \text{ , } l\text{]}\end{array} \quad = \frac{n}{2B}\hat{C}_{4,l,k_l,k_r}^{\mathrm{sub},(1)} \quad (50)$$

and the corresponding non-complete diagrams are

$$\hat{D}_{4a,l,k_l,k_r}^{(1)} = \quad \begin{array}{c}\text{[diagram: } \tfrac{n}{2}-l \text{ , } l\text{]}\end{array} \quad = \frac{n}{2B}\hat{C}_{4a,l,k_l,k_r}^{(1)}$$

$$\hat{D}_{4b,l,k_l,k_r}^{(1)} = \quad \begin{array}{c}\text{[diagram: } \tfrac{n}{2}-2-l \text{ , } l\text{]}\end{array} \quad = \frac{n}{2B}\hat{C}_{4b,l,k_l,k_r}^{(1)}.$$

$$(51)$$

Here we need two indices $k_{l,r}$ to account for the positions of the two turning points which makes counting quite cumbersome. Luckily for fixed values of $k_{l,r}$ and l one can show that the contribution of this family vanishes due to multiple counting if all quasi-spin factors are the same. The argument is analogous to the third family.

The same argument also cancels the contribution of the fifth family with the complete sub-diagrams

$$\hat{D}_{5,l,k}^{\mathrm{sub},(1)} = \quad \begin{array}{c}\text{[diagram: } \tfrac{n}{2}-2-l \text{ , } l\text{]}\end{array} \quad = \frac{n}{2B}\hat{C}_{5,l,k}^{\mathrm{sub},(1)}. \quad (52)$$

In this diagram $\frac{n}{2} - l - 2$ must be odd and the diagrams with $1 < l < \frac{n}{2} - 3$ to give a new diagram. The corresponding non-complete diagrams are

$$\hat{D}_{5a,l,k}^{(1)} = \quad \begin{array}{c}\text{[diagram: } \tfrac{n}{2}-l \text{ , } l\text{]}\end{array} \quad = \frac{n}{2B}\hat{C}_{5a,l}^{(1)}$$

$$\hat{D}_{5b,l,k}^{(1)} = \quad \begin{array}{c}\text{[diagram: } \tfrac{n}{2}-2-l \text{ , } l\text{]}\end{array} \quad = \frac{n}{2B}\hat{C}_{5b,l,k}^{(1)}.$$

$$(53)$$

All non-trivial contributions to the first-order form factor come from the two remaining families of diagrams. They contain no turning point but do contain loops of antiparallel lines. The complete diagrams of the sixth family

$$\hat{D}_{6,l}^{\mathrm{sub},(1)} = \quad \begin{array}{c}\text{[diagram: } \tfrac{n}{2}-2-l \text{ , } l\text{]}\end{array} \quad = \frac{n}{2B}\hat{C}_{6,l}^{\mathrm{sub},(1)} \quad (54)$$

contain one parallel and one anti-parallel loop while the complete diagrams

$$\hat{D}_{7,l}^{\mathrm{sub},(1)} = \quad \begin{array}{c}\text{[diagram: } \tfrac{n}{2}-2-l \text{ , } l\text{]}\end{array} \quad = \frac{n}{2B}\hat{C}_{7,l}^{\mathrm{sub},(1)} \quad (55)$$

of the seventh family contain two anti-parallel loops. In both types of complete diagrams l is odd. In the sixth

family $\frac{n}{2} - 2 - l$ is even while it is odd in the seventh family. Thus the sixth family only exists for odd $\frac{n}{2}$ and the seventh only for even $\frac{n}{2}$. If $l = 1$ the diagrams $D_{6,1}^{\text{sub},(1)}$ and $D_{7,1}^{\text{sub},(1)}$ are the same as $D_{2,1,k}^{\text{sub},(1)}$ (with k such that the turning point is on the scattering region in the right loop). For $l = \frac{n}{2} - 2$ the diagram $D_{6,\frac{n}{2}-2}^{\text{sub},(1)}$ is the same as $D_{1,\frac{n}{2}-2}^{\text{sub},(1)}$. Thus for the sixth family $l = 3, 5, \ldots, \frac{n}{2} - 4$ which gives $\frac{1}{2}(\frac{n}{2} - 5)$ different diagrams. In the seventh family the diagrams $D_{7,l}^{\text{sub},(1)}$ are the same as $D_{7,\frac{n}{2}-2-l}^{\text{sub},(1)}$ such that $l = 3, 5, \ldots, \frac{n}{4} - 2$ (or $l = 3, 5, \ldots, \frac{n}{4} - 1$) if $\frac{n}{4}$ is odd (even) which gives $\frac{1}{2}(\frac{n}{4} - 3)$ (or $\frac{1}{2}(\frac{n}{4} - 1)$) different diagrams. If $\frac{n}{4}$ is even and $l = \frac{n}{4} - 1$ the multiplicity factor should be $\frac{n}{4}$ instead of $\frac{n}{2}$ as given in the formula above. In both cases the sum of the multiplicity factors over all different diagrams is $\frac{n}{4}(\frac{n}{4} - 3)$ for the seventh family.

The non-complete diagrams of the sixth and seventh families are given by

$$\hat{D}_{6a,l}^{(1)} = \quad [\text{diagram}] \quad = \frac{n}{2B}\hat{C}_{6a,l}^{(1)}$$

$$\hat{D}_{6b,l}^{(1)} = \quad [\text{diagram}] \quad = \frac{n}{2B}\hat{C}_{6b,l}^{(1)} \qquad (56)$$

and

$$\hat{D}_{7a,l}^{(1)} = \quad [\text{diagram}] \quad = \frac{n}{2B}\hat{C}_{7a,l}^{(1)}$$

$$\hat{D}_{7b,l}^{(1)} = \quad [\text{diagram}] \quad = \frac{n}{2B}\hat{C}_{7b,l}^{(1)}. \qquad (57)$$

In both families l is odd while $\frac{n}{2}$ is odd (even) in the sixth (seventh) family. The diagrams $D_{6a,1}^{(1)}$, $D_{6a,3}^{(1)}$, $D_{6a,\frac{n}{2}-2}^{(1)}$, $D_{6b,1}^{(1)}$, $D_{6b,\frac{n}{2}-2}^{(1)}$, $D_{7a,1}^{(1)}$, $D_{7a,3}^{(1)}$ and $D_{7b,1}^{(1)}$ are not new (they can be found among $D_{1a/1b,l}^{(1)}$ and $D_{2a/2b,l,k}^{(1)}$). Thus $l = 5, 7, \ldots, \frac{n}{2} - 4$ (or $l = 3, 7, \ldots, \frac{n}{2} - 4$) for $D_{6a,l}^{(1)}$ ($D_{6b,l}^{(1)}$) which gives $\frac{1}{2}(\frac{n}{2} - 7)$ (or $\frac{1}{2}(\frac{n}{2} - 5)$) new diagrams in the sixth family.

For odd (even) $\frac{n}{4}$ the multiplicity factor of the diagram $D_{7a,\frac{n}{4}}^{(1)}$ ($D_{7b,\frac{n}{4}-1}^{(1)}$) for is reduced to $\frac{n}{4}$ due to the symmetry of these diagrams. If $\frac{n}{4}$ is odd (even) $l = 5, 7, \ldots, \frac{n}{4} - 2$ (or $l = 3, 5, \ldots, \frac{n}{4} - 3$) for the diagrams $D_{7a,l}^{(1)}$ ($D_{7b,l}^{(1)}$) and the sum over the multiplicities is $\frac{n}{4}(\frac{n}{4} - 4)$ (or $\frac{n}{4}(\frac{n}{4} - 2)$).

Assuming that within each family the quasi-spin factors have all the same value $C_{6,7}^{(1)}$ almost all diagrams

in the sixth and seventh families are canceled by sub-diagrams in the corresponding families. The mechanism is similar to the third, fourth, and fifth family. The main difference is that some of the sub-diagrams in the sixth and seventh family also appear as sub-diagrams in the first and second families of diagrams which leads to additional overcounting. Each of the sub-diagrams actually appears three times as a sub-diagram – e.g. $D_{6,l}^{\text{sub},(1)}$ for $\frac{n}{2} - 6 \geq l \geq 5$ is sub-diagram of $D_{6a,l}^{(1)}$, $D_{6a,l-2}^{(1)}$ and $D_{6b,l}^{(1)}$ thus each has been overcounted twice. The sum over all diagrams with corresponding corrections due to overcounting gives

$$\sum_l D_{6a,l}^{(1)} + \sum_l D_{6b,l}^{(1)} - 2\sum_l D_{6,l}^{\text{sub},(1)} = -\frac{n}{2B}C_6^{(1)} \quad (58\text{a})$$

$$\sum_l D_{7a,l}^{(1)} + \sum_l D_{7b,l}^{(1)} - 2\sum_l D_{7,l}^{\text{sub},(1)} = -\frac{n}{4B}C_7^{(1)}, \quad (58\text{b})$$

where the contribution of the sixth family only exists for odd $\frac{n}{2}$ and the contributions of the seventh family only for even $\frac{n}{2}$. These will be responsible for the leading order beyond the self-dual approximation in all seven ensembles.

2. The Andreev class C

In class C there are no additional spin-components of the wave function. The ensemble average leads to the condition that every scattering region has as many incoming electron lines as hole lines and $C = \pm 2$ for all quasi-spin factors. The sign is positive for even $\frac{n}{2}$ and negative for odd $\frac{n}{2}$ (two d-vertices within a scattering region carry a factor -1) while the factor two corresponds to interchanging electron and hole lines. In the self-dual approximation only the diagram $D_1^{(0)} = -2$ fulfills the stated condition which leads to

$$K_{1,n} = \begin{cases} 0 & n = 2s+1 \\ 0 + \mathcal{O}(\frac{1}{B}) & n = 4s \\ -4 + \mathcal{O}(\frac{1}{B}) & n = 2(2s+1) \end{cases} \quad (59)$$

where s is some integer. Time-averaging gives the correct leading order $K_1(\tau) = 1 + \mathcal{O}(\tau)$. In the next order all diagrams in the first five families are canceled due to overcounting since the quasi-spin factors are equal while in the sixth and seventh family (and also some among the other five) each diagram contains at least one loop with antiparallel lines. Along these any scattering region has two incoming lines of the same type. thus they do not survive the ensemble average and we have $K_1(\tau) = 1 + \mathcal{O}(\tau^2)$ as predicted by random-matrix theory (42).

3. The Andreev class CI

In class CI the quasi-spin factors are the same as for class C as no spin is present. The ensemble average leads

to the weaker condition that every scattering region contains an even number of d-vertices. In the self-dual approximation thus both diagrams contribute. In the next to leading order only the contribution from the sixth and seventh family contribute. Altogether this gives

$$K_{1,n} = \begin{cases} 0 & n = 2s + 1 \\ 2n - \frac{n}{B} + \mathcal{O}(\frac{1}{B^2}) & n = 4s \\ -4 - 2n + \frac{2n}{B} + \mathcal{O}(\frac{1}{B^2}) & n = 2(2s+1). \end{cases} \quad (60)$$

Since $\tau = \frac{n}{2B}$ time averaging yields $K_1(\tau) = -1 + \frac{\tau}{2} + \mathcal{O}(\tau^2)$ in accordance with the random-matrix theory result (42)..

4. The Andreev class D

In class D we have to take the spin components into account. The ensemble average lead to a set of conditions on the scattering regions. It will suffice to consider one large complete open loop to identify all allowed configurations. The complete open loops can be obtained from the two self-dual diagrams by cutting two (anti-)parallel lines. We will neglected contributions which are exponentially suppressed in the limit $n, B \to \infty$. First consider an anti-parallel loop and put either two parallel or two anti-parallel spins on two anti-parallel lines. For anti-parallel lines with parallel spins both spins are always flipped from one side of the scattering region to the other. Anti-parallel spins on anti-parallel lines are never flipped. In both cases we can only choose the spins on one pair of parallel lines and the spins on *all* lines in the loop are fixed. Since ever scattering region carries a factor $\pm \frac{1}{2}$ any configuration with anti-parallel lines is suppressed exponentially with a factor 2^{-m} for a loop of length m.

In a loop of parallel lines the situation is different. Only configurations of parallel spins on parallel lines survive the ensemble average. However the spins may either flip or not when parallel lines hit a scattering region. Since there are 2^m such configurations on a loop with m scattering regions and $2m$ lines, the factor 2^{-m} of the scattering regions is canceled (in this configuration the factor from each scattering region is positive). For a loop we thus have the same conditions on a scattering region as in class C. Only the diagrams $D_1^{(0)}$, $D_{1b,l}^{(1)}$, $D_{3a,l}^{(1)}$ and $D_{3b,l}^{(1)}$ fulfill this condition. However, the contributions of the first and third families have been shown to vanish under the given conditions such that contributions to the order τ remain. Altogether

$$K_{1,n} = 2\langle s_n \rangle = \begin{cases} 0 & n = 2s + 1 \\ 0 + \mathcal{O}(\frac{1}{B^2}) & n = 4s \\ 4 + \mathcal{O}(\frac{1}{B^2}) & n = 2(2s-1) \end{cases} \quad (61)$$

and time averaging yields the corresponding result from random-matrix theory $K_1(\tau) = 1 + \mathcal{O}(\tau^2)$ upto the order we have calculated (42).

5. The Andreev class DIII

After the ensemble average in class DIII the the spins have to be parallel in a parallel loop where the scattering regions carry a positive factor $\frac{1}{2}$. In consequence, the first self-dual diagram has the value $D_1^{(0)} = 2$ as the quasi-spin factor is $C^{(0)} = 2\,2^{\frac{n}{2}}2^{-\frac{n}{2}} = 2$. For an anti-parallel loop only configurations with anti-parallel spin need to be counted (the sum over some remaining contributions is exponentially suppressed). At any scattering region the spins may then either flip or not – every time they both flip the scattering region carries a negative sign (else the factor is positive). A turning point inside a loop has anti-parallel spins on two connected lines and always carries a positive sign whatever allowed spin configuration on both sides. As a consequence, for any quasi-spin configuration that contributes to $D_2^{(0)}$ there is another configuration with opposite sign which has a different spin on one pair of lines connected to the turning point region. We thus have $D_2^{(0)} = 0$. The same is true for any diagram which contains a turning point.

The argument for the cancellation of almost all diagrams but the contributions given in equations (58a) and (58b) in the preceeding section assumed the same quasi-spin factor for all diagrams. It can be generalized to class DIII (and also all other classes) if one properly only subtracts those quasi-spin configurations in the subdiagrams that actually have been overcounted (the subdiagrams may contain allowed configurations that have been counted properly). The overcounted configurations that appear in the quasi-spin factors $C_{6,7}^{(1)}$ are the corresponding quasi-spin factors of the diagrams $D_{6a,l}^{(1)}$ and $D_{7a,l}^{(1)}$. For configurations that contribute to $C_6^{(1)}$ the number of spin flips in the left loop is necessarily positive which gives a positive sign to each contribution. Altogether one gets $C_6^{(1)} = 1$. Indeed, all the scattering regions give a factor $2^{-\frac{n}{2}}$, the electron-hole interchange gives a factor 2 and the spins $2^{\frac{n}{2}-1}$ (the spins on the four lines connecting the two loops are determined by a single spin index). The other quasi-spin factor is $C_7^{(1)} = -1$. The different sign is due to an odd number of spin flips along both anti-parallel loops here. The complete result for the form factor $K_{1,n} = \langle s_n \rangle$ is

$$K_{1,n} = \begin{cases} 0 & n = 2s + 1 \\ -\frac{n}{2B} + \mathcal{O}(\frac{1}{B^2}) & n = 4s \\ 2 + \frac{n}{4B}\mathcal{O}(\frac{1}{B^2}) & n = 2(2s+1) \end{cases}. \quad (62)$$

As $\tau = \frac{n}{2B}$ time averaging yields $K_1(\tau) = \frac{1}{2} - \frac{\tau}{8} + \mathcal{O}(\tau^2)$ which is again the corresponding random-matrix theory result (42).

6. The chiral class AIII

Parallel loops do not survive the ensemble average in the chiral class AIII. Thus the first self-dual diagram vanishes $D_1^{(0)} = 0$. Long loops with anti-parallel lines only have weight if the spins are always parallel. At each scattering region they may either flip or not – in both cases the scattering region carries a positive factor. Turning points inside a loop carry a negative sign if the two incoming lines have opposite spin, else the sign is positive. By flipping spins on one side of a turning point one can thus change the overall sign of a configuration. Eventually all diagrams with a turning point vanish. There is no contribution at all to the self-dual approximation. Among all diagrams that contribute to the linear order only the seventh family has to be considered – all other diagrams either contain a turning point or a long loop of parallel lines or they cancel due to overcounting. In equation (58b) the factor $C_7^{(1)}$ is the quasi-spin factor of the diagrams $D_{7,l}^{(1)}$ which is $C_7^{(1)} = 1$. Altogether we have

$$K_{1,n} = \begin{cases} 0 & n = 2s + 1 \\ 0 + \mathcal{O}(\frac{1}{B^2}) & n = 4s \\ -\frac{n}{2B} + \mathcal{O}(\frac{1}{B^2}) & n = 2(2s+1). \end{cases} \quad (63)$$

Here $\tau = \frac{n}{4B}$ such that time averaging gives the form factor $K_1(\tau) = -\frac{\tau}{2} + \mathcal{O}(\tau^2)$ as predicted by random-matrix theory (42).

7. The chiral class BDI

In the next chiral class, BDI long loops of parallel lines survive the ensemble average in addition to the anti-parallel loops of class AIII. For loops of parallel lines all scattering regions carry a positive sign. For anti-parallel loops and turning points the discussion of class AIII can be taken over completely. The only additional contributions to the form factor are due to the first self-dual diagram $D_1^{(0)} = 2$ and due to the contribution (58a) of the sixth family of diagrams for the linear order. Here, $C_6^{(1)} = 1$ and we arrive at

$$K_{1,n} = \begin{cases} 0 & n = 2s + 1 \\ 0 - \frac{n}{2B} + \mathcal{O}(\frac{1}{B^2}) & n = 4s \\ 4 - \frac{n}{B} + \mathcal{O}(\frac{1}{B^2}) & n = 2(2s+1) \end{cases}. \quad (64)$$

Again, with $\tau = \frac{n}{4B}$ and time averaging we get the random-matrix result (42) $K_1(\tau) = 1 - \frac{3\tau}{2} + \mathcal{O}(\tau^2)$.

8. The chiral class CII

Finally, in class CII the discussion is almost equivalent to the preceeding. Loops of parallel lines have anti-parallel spins and in such a loop a scattering region carries a negative sign if both spins flip. In conclusion $D_1^{(0)} = -2$ since an odd number of spin flips occurs. For anti-parallel lines the spins are always parallel and the scattering regions carry a positive sign. Turning points inside such a loop can have either sign. For $C_6^{(1)}$ the number of spin flips along the parallel loop is always even, thus $C_6^{(1)} = C_7^{(1)} = 1$ and we have

$$K_{1,n} = \begin{cases} 0 & n = 2s + 1 \\ 0 - \frac{n}{4B} + \mathcal{O}(\frac{1}{B^2}) & n = 4s \\ -2 - \frac{n}{2B} + \mathcal{O}(\frac{1}{B^2}) & n = 2(2s+1). \end{cases} \quad (65)$$

Here, $\tau = \frac{n}{2B}$ and the time average yields $K_1(\tau) = -\frac{1}{2} - \frac{3\tau}{8} + \mathcal{O}(\tau^2)$. Needles to say this is in accordance with the random-matrix theory prediction (42).

IV. CONCLUSION

We have given a systematic diagrammatic short-time expansion of the first-order and second-order form factors for ensembles of star graphs in the ten symmetry classes. The leading orders (diagonal and self-dual approximations) have been calculated explicitly along with the first order beyond. The fidelity to the predictions of Gaussian random-matrix ensemble has been established to this order. These results support the proper generalization of the Bohigas-Giannoni-Schmit conjecture to the novel symmetry classes. The contributing diagrams for the ensembles of star graphs can be expected to carry over to Hamiltonian flows. For magnetic Andreev billiards in class C this is indeed the case [12]. For more general flows in all novel classes a description of the self-dual approximation will be given in a future work [20]. A theory for flows beyond the self-dual approximation for the novel ensembles will follow the paths of the Sieber-Richter theory for time-reversal invariant Wigner-Dyson systems. The results given here for quantum graphs are however more systematic as the existing work on Wigner-Dyson flows as we could show that no other contributions exist that contribute to the calculated order of the form factors.

[1] O. Bohigas, M.J. Giannoni, and C. Schmit, Phys. Rev. Lett. **52**, 1 (1984).

[2] T. Guhr, A. Müller-Groeling, and H.A. Weidenmüller, Phys. Rep. **299**, 189 (1998).

[3] F. Haake, *Quantum Signatures of Chaos* (2nd edition, Springer, Berlin, 2000).

[4] M.C. Gutzwiller, J. Math. Phys. **12**, 343 (1971)

[5] M.V. Berry, Proc. R. Soc. Lond. A **400**, 299 (1985).

[6] M. Sieber, and K. Richter, Phys. Scr. T **90**, 128 (2001); M. Sieber, J. Phys. A **35**, L613-L619 (2002).

[7] S. Müller, Diploma thesis (Essen 2001); S. Müller, Eur. Phys. J. B **34**, 305 (2003).

[8] D. Spehner, J. Phys. A **36**, 7269 (2003).

[9] M. Turek and K. Richter, J. Phys. A **36**, L455 (2003).

[10] S. Müller, K. Richter, D. Spehner, and M. Turek, to be published

[11] S. Heusler, S. Müller, P. Braun, and F, Haake, arxiv:nlin.CD/0309022.

[12] S. Gnutzmann, B. Seif, F. von Oppen, and M. Zirnbauer, Phys. Rev. E **67**, 046225 (2003).

[13] G. Berkolaiko, H. Schanz, and R.S. Whitney, Phys. Rev. Lett. **88**, 104101 (2002); G. Berkolaiko, H. Schanz, R.S. Whitney, arXiv:nlin.CD/0205014 (2002); G. Berkolaiko, arxiv:nlin.CD/0305009.

[14] S. Heusler, J. Phys. A **34**, L483 (2001).

[15] J. Bolte, and J. Harrison, J. Phys A **36**, L433 (2003);J. Bolte, and J. Harrison, J. Phys A **36**, 2747 (2003).

[16] S. Gnutzmann, and B. Seif, to be published; B. Seif, dissertation thesis (Köln 2003).

[17] F. Barra and P. Gaspard, J. Stat. Phys. **101**,283 (2000).

[18] T. Kottos and U. Smilansky, Phys. Rev. Lett **79**, 4794 (1997); Ann. Phys. **274**, 76 (1999).

[19] G. Berkolaiko, and J.P. Keating, J. Phys. A **32**,7827 (1999); G. Berkolaiko, E.B. Bogomolny, and J.P. Keating, J. Phys. A **34**, 335 (2001).

[20] S. Gnutzmann, to be published.